Genome-wide analysis reveals pathways important for the development and maturation of excitatory synaptic connections to GABAergic neurons

Devyn B. Oliver[1,3], Shankar Ramachandran[1], Kasturi Biswas[1,3], Hailey McKillop[2], Noelia Genao[2], Michele L. Lemons[1,2], Michael M. Francis[1,3*]

[1] Department of Neurobiology, University of Massachusetts Chan Medical School, Worcester, MA, U.S.A

[2] Department of Biological and Physical Sciences, Assumption University, Worcester, MA, U.S.A.

[3] Program in Neuroscience, University of Massachusetts Chan Medical School, Worcester, MA

*Corresponding author: Michael.Francis@umassmed.edu

Keywords: *C. elegans*, acetylcholine receptor, trafficking, synapse, active zone, dendritic spine

Abstract

A high degree of cell and circuit-specific regulation has presented challenges for efforts to precisely define molecular mechanisms controlling synapse formation and maturation. Here, we pursue an unbiased forward genetic approach to identify *C. elegans* genes involved in the formation and maturation of cholinergic synaptic connections with GABAergic motor neurons as indicated by the distribution of GFP-tagged postsynaptic AChRs in GABAergic dendrites. We identified mutations in 3 genes that identify key processes in synapse/circuit maturation: postsynaptic receptor assembly, cargo trafficking, and synapse structural organization. Mutation of the RUN domain (RPIP8, UNC-14, and NESCA) cargo adaptor *unc-14* dramatically impacted both dendritic spines and overall GABAergic neuron morphology. In contrast, mutation of the nicotinic acetylcholine alpha subunit *unc-63* caused a failure in AChR assembly in GABAergic neurons but did not significantly alter dendritic spine structure or abundance. Notably, specific expression of wild type *unc-14* cDNA in either GABAergic neurons or presynaptic cholinergic neurons was not sufficient to rescue the *unc-14* mutant phenotype while pan-neuronal expression provided significant rescue, indicating that disruptions in GABAergic neuron morphology arise from compound effects. Finally, we obtained a mutation in the Liprin-α synaptic scaffold *syd-2* that produces a stop codon in a C-terminal SAM domain and has severe effects on dendritic spines and AChR localization. Our unbiased strategy identified key genes that implicate three distinct cellular processes important for synapse/circuit development and maturation. The identification of these genes from our screen highlights how mechanisms for receptor assembly, cargo trafficking and synapse structural organization each contribute to circuit connectivity.

Acknowledgments

We would like to acknowledge Christopher Lambert and Julia Russell for their contributions in building molecular reagents and worm strains, Andrea Thackeray for helping with EMS mutagenesis, and Claire Benard and Maria Doitsidou for bioinformatic analysis. CRISPR/Cas9 engineered mutations were designed and produced by Paola Perrat and Peng Ding from the University of Massachusetts Chan Medical School CRISPR CORE. This research was supported by NINDS RO1NS064263 (MMF), NSF IOS1755019 (MMF), NSF IOS1754986 (MLL) and NIH F31NS103365 (DBO).

Author contributions

DBO screened for mutants, isolated candidates, performed variant discovery outcross mapping, extracted the DNA used for whole genome sequencing (WGS), identified the causal mutation in the isolated mutants, and characterized each candidate. SR performed Ca^{2+} imaging experiments, analysis and assisted with preparing the manuscript. KB performed strain building, behavior experiments, imaging and analysis. HK and NG built strains, performed behavior experiments and analysis. MLL performed behavior experiments and data analysis. MMF was responsible for project conceptualization and writing the manuscript.

Competing interests

No competing interests declared

Introduction

Nervous system performance relies on precise organization of synaptic connections between neurons. Both presynaptic and postsynaptic machinery must be properly trafficked to nascent sites of synaptic contacts and stabilized. Presynaptic protein complexes recruit neurotransmitter-filled synaptic vesicles to specific sites, known as active zones (AZ), and neurotransmitter receptors are clustered at high density in apposition to these AZs. Specific neurotransmitter receptor types are localized in a cell- and synapse-type specific manner, based at least in part on their subunit composition. While we now have generalized knowledge of the various processes that guide these steps in synapse development, the molecular mechanisms involved often show a high degree of cell-type specificity, complicating efforts to gain a comprehensive mechanistic understanding of synapse development processes across neuron classes and neurotransmitter systems.

Genome-wide screening approaches in invertebrates have proven particularly valuable for identifying conserved genetic pathways involved in synapse formation. In *C. elegans*, these efforts have largely focused on the identification of genes involved in the organization of neuromuscular synapses. For example, screens to identify mutants with mislocalized synaptic vesicle markers at GABAergic neuromuscular synapses identified conserved genes such as *syd-2* that encode presynaptic scaffolds important for active zone structural organization (Yeh et al., 2005). Additionally, screens to identify mutants resistant to the effects of the nAChR agonist levamisole identified extracellular scaffold genes important for the clustering of muscle AChRs at cholinergic neuromuscular synapses (Chaya et al., 2021; Jospin et al., 2022). By comparison, molecular mechanisms critical for the formation of synapses onto *C. elegans* neurons are less well defined. Our previous work showed that the presynaptic adhesion protein NRX-1 stabilizes developing spines on postsynaptic GABAergic dendrites (Philbrook et al., 2018; Oliver et al., 2022). However,

additional players in the development of spines and their associated postsynaptic sites have remained unidentified.

In this study, we pursued a genome-wide screening approach to obtain mutants in which the organization of postsynaptic cholinergic receptor clusters (AChRs) on GABAergic motor neurons is disrupted. From this screen, we obtained three mutants that indicate molecular mechanisms important for the development and maturation of excitatory synaptic contacts localized to dendritic spines on GABAergic motor neurons. We isolated a new mutant allele of the nicotinic receptor alpha subunit *unc-63* that disrupts localization of ACR-12 receptor clusters in GABAergic dendrites, providing evidence that UNC-63 is an obligate component of ACR-12-containing receptors. Further, we isolated a new mutant allele of the *unc-14* gene that disrupts both synaptic organization and dendrite outgrowth. *unc-14* encodes a RUN domain adaptor protein previously implicated in cargo selection and trafficking (Sakamoto et al., 2005). Finally, we isolated a new allele of the synaptic scaffold syd-2/Liprin-α, previously shown to be important for the organization of presynaptic sites (Dai et al., 2006), that disrupts the outgrowth of dendritic spines and the clustering of postsynaptic receptors in GABAergic neurons. Our evidence linking these genes with synapse formation in *C. elegans* GABAergic neurons advances a new model for analysis of their functional contributions.

Materials and Methods

Strain maintenance

All strains used are derivatives of N2 Bristol and maintained at room temperature. Animals were grown on nematode growth media plates (NGM) seeded with *E. coli* strain OP50. A complete list of all strains used are found in Table 1.

EMS mutagenesis, whole-genome sequencing and bioinformatic data analysis

To identify genes important for the development or maintenance of synapses onto GABAergic neurons, we conducted a semi-clonal F2 forward screen (Brenner, 1974; Jorgensen and Mango, 2002) to obtain mutants where the clustering of GFP-tagged ACR-12 receptors is disrupted. Transgenic animals stably expressing P*flp-13*::ACR-12::GFP were mutagenized for 4 hours using 25 μM EMS following standard protocols (Brenner, 1974; Jorgensen and Mango, 2002). Mutagenized L4/young adults were transferred to NGM plates. 3-4 days later, F1s were transferred (2/plate) to 50 plates (100 F1s). From each of the 50 F1 plates, 8 F2s were transferred to 4 new plates (2/plate) yielding 400 F2s on 200 plates. L4 stage F2 progeny were screened for disruptions in ACR-12::GFP clustering in DD neurons (absent, displaced, ectopic, decrease or increased number) by spinning disk confocal microscopy.

Candidate mutants were mapped by variant discovery mapping as previously described (Doitsidou et al., 2016). Briefly, mutant phenotypes were first confirmed in subsequent generations. Confirmed candidates were then backcrossed to the starting, non-mutagenized strain carrying P*flp-13*::ACR-12::GFP. Homozygous F2 progeny from 16-23 backcrossed recombinants were pooled for DNA extraction (Qiagen Gentra Puregene Kit) and whole genome sequencing. Homozygous variants within the mapped region were included in the final candidate

list (Doitsidou et al., 2016). Raw sequence data was processed using Galaxy/Cloudmap mapping, subtracting, and filtering pipelines (Minevich et al., 2012). Sequence reads were aligned to the reference genome (wild type/N2 Bristol) using the fast short read Burrows-Wheeler Aligner (BWA). For high coverage and high-quality datasets only reads with a Phred score of >30 (according to FastQC) for each base pair was used. Variants were identified using GATTK Unified Genotyper from the GATK suite. Variations present in the P*flp-13*::ACR-12::GFP starting strain were subtracted and filtered (read depth of ≥3) from the mutant sequence results using GATK SelectVariants from the GATK suite. Variants were plotted using CloudMap and annotated using SnpEff.

Imaging and fluorescent quantification

L4 animals were immobilized with sodium azide (0.3 M) on 2% or 5% agarose pads. Z-stack confocal volumes were obtained using a Yokogawa CSU-X1 spinning disk confocal mounted on an Olympus BX51WI upright microscope equipped with a Hamamatsu EM-CCD camera and 63x oil immersion objective. Analysis of synapse number and fluorescence intensity was performed using FIJI ImageJ software (Schindelin et al., 2012) using defined threshold values acquired from control experiments for each fluorescent marker. Statistical analysis for all synaptic and spine analysis between two groups utilized a student's t-test; for comparisons of multiple groups, one-way or two-way ANOVA was used with the appropriate post hoc test.

Molecular biology

Plasmids were constructed using the two-slot Gateway Cloning system (Invitrogen) and confirmed by restriction digest and sequencing. All plasmids and primers used in this work are described in Table 2.

CRISPR/Cas9 design and gene editing

The Bristol N2 strain was used as the wild-type strain for all CRISPR/Cas9 editing. *unc-63* and *syd-2* gene editing was performed by CRISPR/Cas9 using established protocols (Arribere et al., 2014). Site-specific sgRNAs and repair template donor ssODNs were manually designed and generated by IDT (Integrated DNA Technologies, Inc.). Injection mixtures were prepared following established protocols (Arribere et al., 2014). Mutations in the *dpy-10* gene were used as a CRISPR co-conversion marker. Base substitutions were confirmed via Sanger sequencing. All crRNAs, ssODNs, and PCR screening sequences are reported in Table 2.

Aldicarb and levamisole assays

Assays were performed on synchronous populations of Day 1 adult animals. At least 10 worms of each genotype were transferred to separate plates containing NGM agar and either 1 mM aldicarb or 250 μM levamisole. The number of paralyzed animals was recorded every 15 minutes and the rate of paralysis was plotted as a function of time using GraphPad Prism. Assays were repeated on at least 3 separate days.

Behavioral assays

Staged day 1 adult animals were placed on behavioral assay plates coated with a thin OP-50 lawn. Following one minute of habituation, worm movement was recorded using the WormLab Imaging System (MBF Bioscience). Post-hoc analysis was performed using the WormLab software. The total length of the worm's movement path (track length), calculated by summing the lengths of all forward and backward movements, over 1-minute duration from the start of image acquisition was calculated. Statistical comparisons were performed by one-way ANOVA with Bartlett's correction using GraphPad Prism.

Calcium imaging

Simultaneous optogenetics and calcium imaging was performed as previously described (Philbrook et al., 2018). Ca^{2+} transients were recorded from muscle cells in transgenic animals co-expressing P*myo-3*::NLSwCherry::SL2::GCaMP6s (muscle, from Mark Alkema) along with P*acr-2*::Chrimson (cholinergic neurons). Animals were placed on plates seeded with OP50 containing 2.75 mM All-Trans Retinal (ATR) for 24 hr prior to experiments. Young adults were immobilized on 5% agarose pads in 2,3-Butanedione monoxime (BDM) (30 mg/ml). For all genotypes, control animals grown in the absence of ATR were imaged.

Data were acquired at 10 Hz sampling using Volocity software. Pre-stimulus baseline fluorescence (F0) was calculated as the average of the corrected background-subtracted data points in the first 4 s of the recording and the corrected fluorescence data was normalized to prestimulus baseline as $\Delta F/F0$, where $\Delta F = F - F0$. Peak $\Delta F/F0$ was determined by fitting a Gaussian function to the $\Delta F/F0$ time sequence using Multi peak 2.0 (Igor Pro, WaveMetrics). All data collected were analyzed, including failures (no response to stimulation). If the data points within the stimulation window could be fitted with a Gaussian function, it was deemed a response. If no fit was possible, then it was a failure. In the case of responses not synchronized with the stimulus, a fit would be possible but the response was not synchronized with the stimulus, so it was scored as a failure. Latency was calculated as the time required from stimulus onset (@ 5s) for fluorescence to reach two times the pre-stimulus baseline standard deviation (Larsch et al., 2015).

Results

A forward screen to identify genes important for neuronal AChR clustering/assembly

To identify genes important for the formation or maintenance of synaptic connections in the *C. elegans* motor circuit, we performed a forward genetic screen to obtain mutants where the clustering and/or distribution of AChRs in dorsal type D class GABAergic motor neurons (DD) is

disrupted. ACR-12-containing AChR clusters are organized into synapses located at the tips of spines in mature DD GABAergic dendrites (Philbrook et al., 2018; Cuentas-Condori et al., 2019). We used the mislocalization of ACR-12::GFP to identify candidate mutants where the formation or maintenance of postsynaptic sites located on spines may be altered. We screened L4 stage F2 progeny of EMS-mutagenized animals stably expressing P*flp-13::*ACR-12::GFP for mutants with either misplaced or altered density of AChR clusters in the dendrites of DD neurons. We screened roughly 3300 haploid genomes and obtained several candidate mutants with defects in AChR ACR-12 localization. In particular, we identified three mutant alleles of note: *uf169*, *uf175* and *uf174*. For each of these mutant alleles, we noted striking decreases in ACR-12::GFP fluorescence in GABAergic dendrites. Using next generation sequencing and variant discovery mapping, we identified the causal mutations in 3 of these candidates and describe our analysis of each below.

A mutation in the *unc-14*/RUN domain cargo adaptor disrupts GABAergic neurite outgrowth and organization

Whole genome sequence analysis and variant discovery mapping of *uf169* mutants revealed a point mutation that introduces an early stop in the first exon of the *unc-14* gene, presumably resulting in a null allele (**Fig.1A-B**). UNC-14 encodes a RUN domain (RPIP8, UNC-14, and NESCA) cargo adaptor protein (Sakamoto et al., 2005). RUN domain-containing proteins associate with small GTPases, motor proteins, and interact with cytoskeletal networks (Yoshida et al., 2011), and are implicated in a variety of cellular signaling pathways and processes, including neuronal development, cell migration, GTPase signaling through Rab and Rap families, and endo- and exocytosis (Callebaut et al., 2001). UNC-14 was previously implicated in the outgrowth of GABAergic axons through interactions with the UNC-51 serine/threonine kinase (Ogura et al., 1997; Ogura and Goshima, 2006) and synaptic vesicle transport through

interactions with kinesin motors UNC-116 and KLC-2 (Sakamoto et al., 2005), but its importance in the extension of GABAergic dendrites and the structural organization of postsynaptic sites has not been previously investigated.

unc-14(uf169) mutants show severely uncoordinated movement (**Fig.1D**), similar to previously characterized *unc-14(e57)* loss-of function mutants (Ogura et al., 1997). Expression of the wild-type *unc-14* coding sequence, under a 2.9 kb promoter region upstream of the *unc-14* start, in *unc-14(uf169)* mutants robustly restored normal movement (**Fig.1E**), supporting that *unc-14(uf169)* is a loss-of-function mutation. Pan-neuronal, but not muscle, expression of wild type *unc-14* was also sufficient to rescue the locomotor deficits of *unc-14(uf169)* mutants (**Fig.1E**), indicating a neuronal requirement. However, specific expression in either GABAergic or cholinergic neurons was not sufficient for behavioral rescue (**Fig.1E**), consistent with a broad neuronal requirement for *unc-14* expression.

We next quantified the effects of the *uf169* mutation on ACR-12::GFP fluorescence. We observed the number of fluorescent receptor clusters is severely reduced in DD GABAergic dendrites of *uf169* mutants (**Fig.1C,F**). We found that dendritic ACR-12::GFP fluorescence is similarly reduced in the DD dendrites of previously characterized *unc-14(e57)* loss-of-function animals (**Fig.1C,F**). The effects of the *uf169* mutation on ACR-12/AChR localization could be rescued by expression of the wild type *unc-14* sequence (2.9 kb promoter). Notably, we also observed an increase in the ACR-12::GFP fluorescence in DD neuronal somas relative to the unmutagenized starting strain (**Fig.1C**), perhaps indicative of impaired trafficking from the soma. To better understand how mutation of *unc-14* impacts AChR localization we examined the morphological features of DD neurons in *unc-14* mutants expressing a P*flp-13*::mCherry transcriptional reporter. We noted severe morphological defects in ventral nerve cord DD neurites, including ectopic branching, large varicosities, and misplaced DD somas in the *uf169* mutant (**Fig.1G-H**). We also noted a significant

reduction in dendritic spines in *unc-14(uf169)* mutants (**Fig.1G-H**); however, given the severe dendrite morphology defects observed in these animals, the reduction in spine number may reflect a generalized *unc-14* requirement in dendrite extension rather than a specific role for UNC-14 in dendritic spine outgrowth. While *unc-14* has previously been shown to play a role in neurite outgrowth and extension (Ogura et al., 1997; Sakamoto et al., 2005), our data suggest a previously uncharacterized and novel role for UNC-14 in postsynaptic receptor trafficking and localization.

A novel mutation in the nAChR alpha subunit gene *unc-63* disrupts ACR-12 AChR clustering in DD motor neurons

uf175 mutants demonstrated a stark and significant reduction in receptor cluster numbers in the GABAergic DD dendritic process (**Fig.2C**). Sequence analysis and mapping of *uf175* mutants revealed a missense mutation in exon 2 of the *unc-63* gene (**Fig.2A-B**). *unc-63* encodes a nicotinic acetylcholine receptor (nAChR) alpha subunit that is expressed in both the nervous system and muscles, and is cell type-specifically incorporated into heteromeric nAChRs of varying subunit composition (Culetto et al., 2004). UNC-63 containing nAChRs sensitive to the nicotinic agonist levamisole (L-AChR) have been well-characterized at the *C. elegans* neuromuscular junction (Culetto et al., 2004; Jones et al., 2011). UNC-63 also contributes to other heteromeric nAChR classes in both cholinergic and GABAergic motor neurons (Culetto et al., 2004). The missense mutation carried by *unc-63(uf175)* mutants introduces a P44L substitution at a highly conserved position in the N-terminal extracellular region of UNC-63 immediately adjacent to amino acids implicated in forming the main immunogenic region (MIR) of the human muscle alpha1 nAChR subunit (**Fig.2B**). The MIR is a major target for autoantibodies in humans suffering from myasthenia gravis (Tzartos et al., 1991). Sequence in this region is thought to be important for mediating the conformational maturation of AChRs during receptor assembly as well as for determining sensitivity to activation by ACh.

ACR-12 AChR clusters in DD neurons of *unc-63(uf175)* mutants are decreased by ~65% compared with wild type **(Fig.2C,F).** Mutant *unc-63(uf198)* animals, carrying the same cCg/cTg P44L mutation engineered by CRISPR/Cas9 genome editing, showed a similar decrease in ACR-12 ACR-12 AChR clusters (**Fig.2C,F),** providing additional evidence that the P44L substitution is the causal mutation. Similar decreases in ACR-12 clustering were also observed in previously characterized *unc-63(ok1075)* animals (**Fig.2C,F)** that carry a deletion in the *unc-63* locus (Philbrook et al., 2018), suggesting the identified *uf175* mutation as well as the CRISPR generated *uf198)* mutation are a severe loss-of-function allele. Cell-specific expression of wild-type *unc-63* in GABAergic neurons of *unc-63(uf175)* mutants rescued the decrease in ACR-12 AChR clusters (**Fig.2D,G**), demonstrating a cell-autonomous requirement for UNC-63 in nAChR assembly and synaptic clustering in DD neurons. This finding is consistent with prior studies implicating UNC-63 as a constituent of ACR-12 containing receptors in GABAergic neurons (Philbrook et al., 2018). In contrast to the severe decrease in AChR clusters, the number of dendritic spines in DD neurons of *unc-63(uf198)* mutants is not appreciably different from wild type (**Fig.2E,H**), consistent with prior work that showing that spine formation and stabilization occurs independently of postsynaptic receptor localization (Philbrook et al., 2018) .

***unc-63(uf198)* is a semi-dominant mutation that disrupts neuromuscular function**

In addition to motor neurons, *unc-63* is strongly expressed in body wall muscles and serves an obligate subunit of heteropentameric postsynaptic levamisole-sensitive L-AChRs at neuromuscular synapses (Culetto et al., 2004). To explore how the P44L substitution may impact classes of UNC-63 containing AChRs in other cell types, we next investigated the function of muscle L-AChRs in *unc-63(uf175/198)* mutants. Our interest in this question was motivated in part by our initial observation that the movement of *unc-63(uf175/198)* animals appeared phenotypically less severely affected compared with strains carrying the previously characterized

unc-63(x37) loss-of-function mutations (Culetto et al., 2004). To investigate this possibility, we used post-hoc analysis of worm locomotion and measured movement velocity (**Fig.4A**). We found that the severe *unc-63(x37)* loss-of-function significantly decreased the movement velocity (**Fig.4A**) as previously reported(Culetto et al., 2004). In contrast, the P44L substitution in *unc-63(uf198)* mutants produced no appreciable decrease in movement velocity (**Fig.4A**). To explore this more deeply, we investigated the effects of *unc-63* mutation in combination with deletion of the *acr-16* gene. *acr-16* encodes another nAChR alpha subunit that forms homomeric iAChRs (N-AChR) that operate in parallel with L-AChRs at muscle synapses (Touroutine et al., 2005). Consistent with prior work (Francis et al., 2005; Touroutine et al., 2005), we found that the movement of *unc-63(x37); acr-16(ok789)* double mutants is severely decreased compared with either wild type or *acr-16(ok789)* single mutants. In contrast, the movement *unc-63(uf198); acr-16(ok789)* double mutants is not significantly decreased (**Fig.4A**), suggesting there may be sufficient muscle L-AChR function in *unc-63(uf198)* mutants to support muscle contraction and near-normal movement.

We next sought to investigate the clustering of L-AChRs at neuromuscular synapses in *unc-63(uf175/198)* animals. We quantified the clustering of L-AChRs in muscles using muscle-specific expression of UNC-29::GFP, an obligate non-alpha subunit of L-AChRs (Gottschalk et al., 2005). The number and fluorescence intensity of muscle L-AChR (UNC-29::GFP) clusters were strikingly decreased in *unc-63(uf198)* mutants compared with control (**Fig.3A-C**). This result suggests that the assembly of muscle L-AChR and GABA neuron ACR-12 AChR complexes are similarly disrupted in *unc-63(uf198)* mutants. However, our observation that movement is not appreciably affected in these animals supports the idea that a low level of receptor assembly persists in *unc-63(uf198)* animals and is sufficient to support muscle contraction and movement.

To further investigate the function of muscle L-AChR in *unc-63(uf198*) animals, we measured the effects of exposure to either the cholinesterase inhibitor aldicarb or the L-AChR agonist levamisole. Wild type animals are paralyzed in response to prolonged treatment with either chemical. The time course over which paralysis occurs is widely used as a measure of cholinergic function. We found that *unc-63(uf198)* animals are strongly resistant to the paralyzing effects of either aldicarb or levamisole, similar to animals carrying the severe *unc-63(x37)* loss-of-function allele (**Fig.3D-G**). Muscle specific expression of wild-type *unc-63* in *unc-63(uf198)* restored paralysis in response to aldicarb treatment; however, only weakly altered paralysis in response to levamisole. Expression of the same transgene in *unc-63(x37)* mutants was sufficient to restore levamisole-induced paralysis (**Fig.3D-G**). Together, our analysis suggests that the P44L substitution in *unc-63(uf198)* mutants may have dominant negative effects, particularly for activation by levamisole. Consistent with this interpretation, we found that *unc-63(uf198)* heterozygous animals had increased resistance to paralysis by aldicarb and levamisole compared with control (**Fig.3D-G**), suggesting *unc-63(uf198)* is a semi-dominant allele.

To investigate cholinergic synaptic responses in *unc-63(uf198)* mutants, we next measured muscle calcium transients evoked by photostimulation of cholinergic motor neurons. To measure muscle calcium responses, we co-expressed the genetically encoded calcium sensor GCaMP6s in muscles with the red-shifted channelrhodopsin Chrimson in cholinergic motor neurons. The cholinergic synaptic response is mediated through both levamisole-sensitive UNC-63-containing AChRs (L-AChR) and levamisole-insensitive ACR-16 AChRs (Francis et al., 2005; Touroutine et al., 2005). Therefore, to focus on muscle calcium responses elicited through L-AChR activation we pursued experiments in *acr-16(ok789)* animals that carry a deletion in the *acr-16* gene. Depolarization of cholinergic motor neurons elicited robust calcium responses in the muscles of wild type control animals that were closely synchronized to the onset of the light stimulus (**Fig.4B-C**). The amplitude of these synchronous calcium responses was dramatically reduced in *unc-*

63(uf198); acr-16(ok789) double mutants compared to either wild type or *acr-16(ok789)* single mutants (**Fig.4B-C**). We observed a similar reduction in these synchronized calcium responses in animals that carried the presumptive null allele *unc-63(x37)* in combination with the *acr-16(ok789)* deletion (**Fig.4C**). Together, these results suggest that *unc-63(uf198)* is a severe reduction-of-function allele. However, we noted another feature of muscle calcium responses in *unc-63(uf198); acr-16(ok789)* animals, many muscles in *unc-63(uf198); acr-16(ok789)* animals displayed large calcium transients that were not closely synchronized to the light stimulus (**Fig.4B**). The frequency of these unsynchronized responses was much higher in *unc-63(uf198); acr-16(ok789)* animals compared with either controls or *unc-63(x37); acr-16(ok789)* animals (**Fig.4D-E**), suggesting this is a unique property conferred by the P44L substitution in *unc-63(uf198)* mutants.

Mutation of *syd-2*/Liprinα disrupts dendritic spine formation

uf174 mutant animals showed decreased receptor cluster number in GABAergic dendrites. Mapping and sequence analysis of a third mutant *uf174* isolated from our forward genetic screen revealed a novel point mutation in the *syd-2* gene (**Fig.5A**). *syd-2* encodes the sole *C. elegans* Liprin-α. *syd-2*/ Liprin-α was first identified as a ligand for LAR family receptor protein tyrosine phosphatases (LAR-RPTP) (Serra-Pagès et al., 1998) and implicated as a structural component of active zones based on a series of elegant genetic studies in *C. elegans* (Zhen and Jin, 1999). The SYD-2/Liprin-a family proteins contain a N-terminal coiled-coil region followed by three C-terminal SAM (sterile-a-motif) domains (**Fig.5A**). The coiled-coil domains are implicated in homo- and hetero-multimerization while the SAM domains form the LH (Liprin Homology) region that binds LAR-RPTP (Serra-Pagès et al., 1998). The *syd-2(uf174)* mutants isolated from the screen carry a C/T missense mutation that produces an early stop at codon 1091 (Q1091stop) of exon 18 that encodes the SAM domain (**Fig.5A**).

ACR-12 AChR clustering was decreased by roughly 50% in *syd-2(uf174)* mutants compared to wild type (**Fig.5B,D**). To obtain additional evidence that the mutation in *syd-2* was causal for the disruption in AChR clustering, we engineered the same mutation in otherwise wild-type animals by CRISPR/Cas9 genome editing. CRISPR/Cas9-engineered *syd-2(uf193)* animals showed similar deficits in AChR clustering to those observed in DD neurons of *syd-2(uf174)* isolated from the screen (**Fig.5B,D**). We next analyzed GABAergic DD dendritic spines (P*flp-13*::mCherry) in *syd-2(uf193)* L4 animals. *syd-2(uf193)* animals have ~65% decrease in the number of DD1 dendritic spines compared to wild type animals (**Fig.5C,E**). These results suggest that, similar to the synaptic adhesion protein NRX-1 (Philbrook et al., 2018; Oliver et al., 2022), SYD-2 may be important for the formation or stabilization of both dendritic spines and ACR-12/AChR clusters at postsynaptic sites. We observed that dendritic spine number was also significantly decreased compared to wild type in available *syd-2* loss-of-function mutants, *syd-2(ju37)* and *syd-2(ok217)* (**Fig.5C,E**). *syd-2(ju37)* animals carry an early stop mutation in sequence encoding SYD-2 the coiled-coil domain while *syd-2(ok217)* animals carry a 2 kb deletion that produces a premature stop(Zhen and Jin, 1999). Pan neuronal expression of wild type *syd-2* cDNA in *syd-2(ok217)* mutants restored spines indicating a neuronal requirement (**Fig.5F**). To further investigate the nature of the *syd-2(uf174/uf193)* mutation, we analyzed the number of GABAergic DD dendritic spines in *syd-2(uf193/+)* heterozygotes. Animals heterozygous for *syd-2(uf193)* had a decreased number of spines compared to wild type, similar to homozygous *syd-2(uf193)* mutants and other homozygous loss-of-function alleles tested (**Fig.5E**), suggesting *uf193* is likely to represent a dominant allele of *syd-2*. SYD-2 has been previously implicated in both presynaptic structural organization and cargo trafficking (Zhen and Jin, 1999; Kittelmann et al., 2013). Our findings newly implicate SYD-2 in the formation or stabilization of postsynaptic receptor clusters and dendritic spines, suggesting presynaptic SYD-2 may act indirectly to coordinate postsynaptic organization. Alternatively, it is possible that a postsynaptic SYD-2 pool contributes to spine

development and the organization of postsynaptic sites. Additional studies will be required to distinguish these possibilities.

Discussion

We pursued an unbiased, genome-wide strategy to elucidate mechanisms directing structural regulation of dendrites and postsynaptic specializations localized to dendritic spines in *C. elegans* GABAergic neurons. We identified 3 genes that, when mutated, disrupt the organization of postsynaptic receptor clusters on GABAergic dendrites. These genes define distinct functional pathways required for establishing synaptic connections: (1) the nAChR subunit UNC-63 is an obligate subunit of postsynaptic receptors and is therefore required for receptor assembly, (2) the RUN domain cargo adaptor UNC-14 is required for dendrite outgrowth, and (3) the synaptic scaffold SYD-2 is required for spine outgrowth or maintenance.

The *unc-14* allele we obtained from our screen generates an early stop codon and is a predicted null. Prior studies of *unc-14* null mutants demonstrated an interaction between *unc-14* and the the S/T kinase UNC-51 and implicated UNC-14 in axonal elongation as well as axonal delivery of a variety of cargoes including synaptic vesicles, the axon guidance cue UNC-6/Netrin, and the Netrin receptor UNC-5 (Ogura et al., 1997; Ogura and Goshima, 2006). Our analysis of dendritic structure revealed striking defects in overall DD dendrite morphology in addition to the disruption of ACR-12/AChR clustering identified from our initial screen. It is therefore unclear whether the defects in postsynaptic organization we observed reflect a requirement for UNC-14 in trafficking post-synaptic components or arise secondarily to a failure in the extension and fasciculation of dendritic processes within the ventral nerve cord. Similar to previous findings for *unc-14(e57)* mutants, we observed bulbous regions in the dendrites of DD GABAergic neurons in *unc-14(uf198)* animals that may represent foci where dendritic material, including post-synaptic proteins, has accumulated due to a failure in trafficking. However, *unc-14* is known to be broadly

expressed in neurons, and our analysis demonstrates that *unc-14* is also expressed in cholinergic motor neurons that lie presynaptic to GABAergic motor neurons. It is therefore also possible that some of the phenotypes we observed in DD dendrites reflect a parallel requirement for *unc-14* in the organization of presynaptic cholinergic axons. Consistent with this hypothesis, we found that *unc-14* expression using either an ~2.5 kb *unc-14* promoter fragment or a pan-neuronal promoter was sufficient to rescue the uncoordinated movement of *unc-14* mutants. In contrast, specific expression in either cholinergic or GABAergic motor neurons was not sufficient to rescue, most consistent with a requirement for *unc-14* expression in both neuron classes for proper motor function.

The P/L substitution mutation in *unc-63* that we isolated disrupts cholinergic receptor clustering in both GABAergic dendrites (P*flp-13*::ACR- 12::GFP) and muscles (P*myo-3*::UNC-29::GFP). The mutation, however, does not affect the formation or maintenance of GABAergic dendritic spines, consistent with prior work demonstrating spine outgrowth independently of receptor clustering (Oliver et al., 2022). Our analysis of *unc-63(uf198)* mutants suggests that proline at this position is important for proper assembly and function of UNC-63-containing AChRs in both muscles and GABAergic dendrites. Prior structural studies of acetylcholine binding proteins from the freshwater snail, *Lymnaea stagnalis* (*L*-AChBP), saltwater mollusk *Aplysia californica*, and the extracellular ligand binding domain of the mouse muscle alpha1 subunit place this residue adjacent to the N-terminal α-helical region at the apical surface of the receptor (Hansen et al., 2004; Albuquerque et al., 2009; Geitmann et al., 2010). Prior mutagenesis studies of chimeric mouse AChRs have implicated this region in receptor assembly and ligand sensitivity (Dash et al., 2014). *C. elegans* mutations that either completely disrupt *unc-63* or alter *unc-63* subunit characteristics have been characterized previously (Culetto et al., 2004). For example, *unc-63(x26)* (C151Y) disrupts the Cys-loop region, a motif important for forming the agonist binding site, and causes a decrease in channel opening frequency. However, cell-specific expression of UNC-63 in this mutant did not change as anti-UNC-63 staining in *unc-63(x26)* animals was similar to wild type (Culetto et al.,

2004), suggesting that *unc-63(x26)* alters channel function but not channel expression. Although the P44L mutation in *unc-63(uf175/uf198)* is not at the ligand binding Cys-loop motif, the proline to a leucine change may likely alter the structure of the extracellular ligand binding domain, impacting the both assembly/folding of UNC-63 subunit and ligand binding.

Given the severe disruption in nAChR clustering we observed and the resistance to pharmacological activation by aldicarb or levamisole, it is surprising that the movement of *unc-63(uf175/uf198)* animals is not more severely disrupted. We conclude the allele is a strong reduction-of-function and residual receptor activity may be sufficient to support relatively normal movement. Our studies of evoked calcium responses in muscles indicate that calcium responses occur in muscles, but these responses are not strictly time-locked to the stimulus. One possibility is that inefficient activation of the receptor may over time produce muscle depolarization. Alternatively, the mutation may indirectly lead to increased spontaneous muscle activity, though a mechanism for such an effect remains unclear. Mammalian ionotropic AChRs are linked with myasthenic syndromes, and nicotine addiction(Léna and Changeux, 1997) while nematode AChRs are common targets for antihelmintic compounds. Our identification and characterization of *unc-63(uf175/uf198)* animals therefore offer additional tools for comparative structure-function studies of this conserved receptor family.

The isolation of a novel *syd-2* allele from our screen newly highlights the importance of this scaffold protein for maintaining postsynaptic organization. Evidence from prior studies across a variety of models implicates SYD-2/Liprin-α as one of several core scaffold proteins responsible for orchestrating presynaptic active zone organization SYD-2/Liprin-α and the rhoGAP domain and PDZ domain-containing scaffold protein, SYD-1, are suggested to localize to nascent active zones in the early stages of presynaptic development, and to subsequently recruit additional presynaptic proteins for presynaptic assembly (Hallam et al., 2002; Dai et al., 2006; Patel et al.,

2006; Fouquet et al., 2009; Owald et al., 2010, 2012; Stigloher et al., 2011; Kittelmann et al., 2013; Spangler et al., 2013; Wentzel et al., 2013; Wong et al., 2018; McDonald et al., 2020; Emperador-Melero et al., 2021). In particular, SYD-1 is suggested to function upstream of SYD-2 and to promote SYD-2 localization and activity at presynaptic sites (Dai et al., 2006; Frankel et al., 2025). Interestingly, *Drosophila dsyd-1*/SYD-1 and *dnrx*/NRX-1 mutants have similar active zone defects and form an *in vivo* complex where dSYD-1 immobilizes neurexin at active zones through a PDZ domain-based interaction (Owald et al., 2012). Similarly, in mammalian neurons, Liprin-α forms a complex with Neurexin1 and another presynaptic scaffold protein Mint1 to regulate the stability of Neurexin1 (LaConte et al., 2016). We showed previously that presynaptic NRX-1/neurexin is required for the maintenance of developing spines, raising the possibility that the postsynaptic alterations we observe in *syd-2* mutants arise secondarily to a mislocalization of NRX-1 at presynaptic sites.

Alternatively, our findings may indicate a postsynaptic requirement for SYD-2. Though less well-characterized compared with its presynaptic roles, immuno-EM studies of rodent cortical neurons have demonstrated that Liprin-α is also localized to postsynaptic sites (Wyszynski et al., 2002). Postsynaptic Liprin-α has been implicated in AMPAR clustering and in shaping morphological features of dendritic spines through interactions with GRIP1 (glutamate receptor-interacting protein 1) and LAR family of receptor protein tyrosine phosphatases (Wyszynski et al., 2002; Dunah et al., 2005; Spangler and Hoogenraad, 2007). Strategies for cell-specific *syd-2* deletion will be required to cleanly dissect potential pre- versus postsynaptic roles for SYD-2/ Liprin-α at synapses onto *C. elegans* GABAergic neurons. However, existing evidence supports predominant presynaptic SYD-2 expression.

Regardless of the precise mechanism of action, the *syd-2(uf174)* and *syd-2(uf193)* alleles offer additional tools for functional analysis of SYD-2 at synapses. Prior work identified a gain-of-function mutation in *syd-2*. *syd-2(ju487)* carries a missense mutation that produces an R/C substitution at position 184 of the conserved LH1 liprin homology 1 domain R184C (Dai et al., 2006). This mutant has synaptic phenotypes opposite to those associated with *syd-2* loss-of-function alleles, including elongated dense core projections, hypersensitivity to the acetylcholine esterase inhibitor aldicarb, and no significant changes in basal or evoked synaptic transmission (Dai et al., 2006; Kittelmann et al., 2013). The mutation we isolated generates an early stop codon in the region encoding the predicted SYD-2 SAM domain. Our observation that the mutation has dominant effects suggests the possibility that a truncated dominant negative SYD-2 protein is produced in which the SAM domain is disrupted, perhaps disrupting the ability of SYD-2 to self-associate.

Collectively, our studies of *unc-14, unc-63,* and *syd-2* offer new avenues for understanding synapse development and organization. Moreover, the novel alleles we isolated from our screen provide new tools for gaining insight into the functions of these genes at synapses.

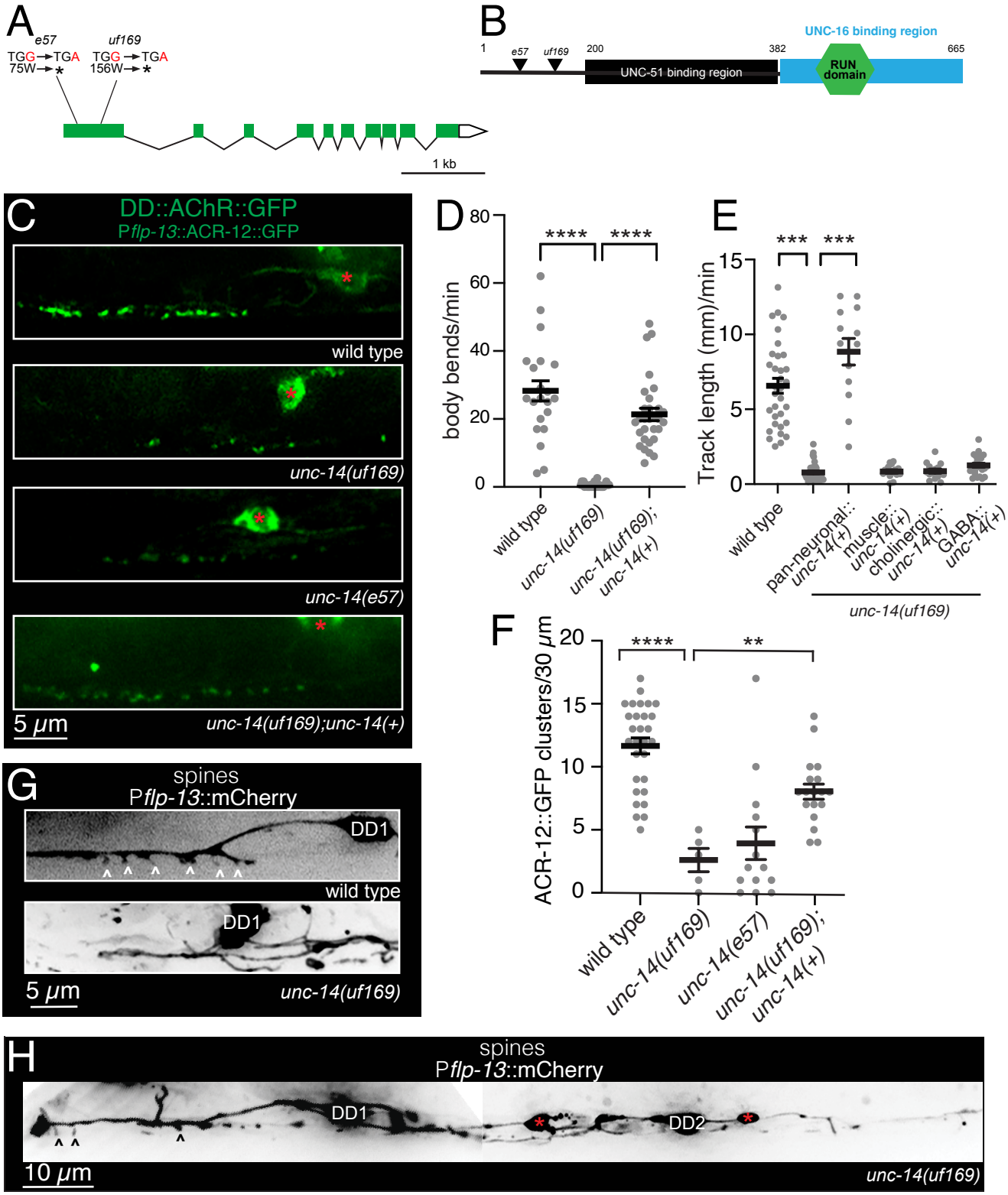
A
e57
uf169
TGG→TGA
75W→*
TGG→TGA
156W→*
1 kb
B
1
e57
uf169
200
382
665
UNC-51 binding region
UNC-16 binding region
RUN domain
C
DD::AChR::GFP
Pflp-13::ACR-12::GFP
wild type
unc-14(uf169)
unc-14(e57)
unc-14(uf169);unc-14(+)
5 μm
D
body bends/min
****
****
wild type
unc-14(uf169)
unc-14(uf169); unc-14(+)
E
Track length (mm)/min
***
***
wild type
pan-neuronal:: unc-14(+)
muscle:: unc-14(+)
cholinergic:: unc-14(+)
GABA:: unc-14(+)
unc-14(uf169)
F
ACR-12::GFP clusters/30 μm
****
**
wild type
unc-14(uf169)
unc-14(e57)
unc-14(uf169); unc-14(+)
G
spines
Pflp-13::mCherry
DD1
wild type
DD1
5 μm
unc-14(uf169)
H
spines
Pflp-13::mCherry
DD1
DD2
10 μm
unc-14(uf169)

Figure 1. *unc-14* mutation disrupts the outgrowth of GABAergic dendrites

A. Transcript of *unc-14*. Reference allele (ef57) and screen isolate allele (*uf169*) mutations are indicated, both resulting in a premature stop (*) in the first exon.

B. UNC-14 protein domains including the predicted binding sites of UNC-16 and UNC-51. Modified from (Sakamoto et al., 2005). Reference allele (e57) and screen isolated allele (uf169) mutations are indicated. Numbers, amino acid positions.

C. Representative confocal images of ACR-12/AChR localization (*Pflp-13*::ACR-12::GFP) in wild type, screen isolate *unc-14(uf169)*, *unc-14(e57)* and genomic rescue of *unc-14(uf169)* animals. Red asterisks, DD1 cell body. Scale bar, 5μm.

D. Quantification of the average body bends per minute in the indicated genotypes. Mean ± SEM. One-way ANOVA with Dunnett's multiple comparison's test. **** $p<0.0001$.

E. Quantification of track length (mm) over 1 min in the indicated genotypes. Mean ± SEM. Motor phenotype was rescued by pan-neuronal *unc-14*(+) expression but not by cholinergic, GABAergic or muscle expression *in unc-14(uf169)* mutant background. One-way ANOVA with Dunnett's multiple comparison's test. *** $p<0.001$.

F. Quantification of the number of ACR-12/AChR clusters in the synaptic region of DD1 dendrite for wild type, screen isolate *unc-14(uf169)*, *unc-14(e57)*, genomic rescue of *unc-14(uf169)* animals. Mean ± SEM. One-way ANOVA with Dunnett's multiple comparison's test, **** $p<0.0001$, ** $p<0.01$.

G. Representative confocal images of DD1 dendrite along the ventral nerve cord (P*flp13*::mCherry) in wild type and *unc-14(uf169)* mutant animals. White carets indicate DD dendritic spines. Scale bar 5μm.

H. Confocal montage images of DD1 and DD2 in *unc-14(uf169)* mutant animals. Black carets point to DD dendritic spines. Red asterisks indicate varicosities along the ventral nerve cord. Scale bar 10μm.

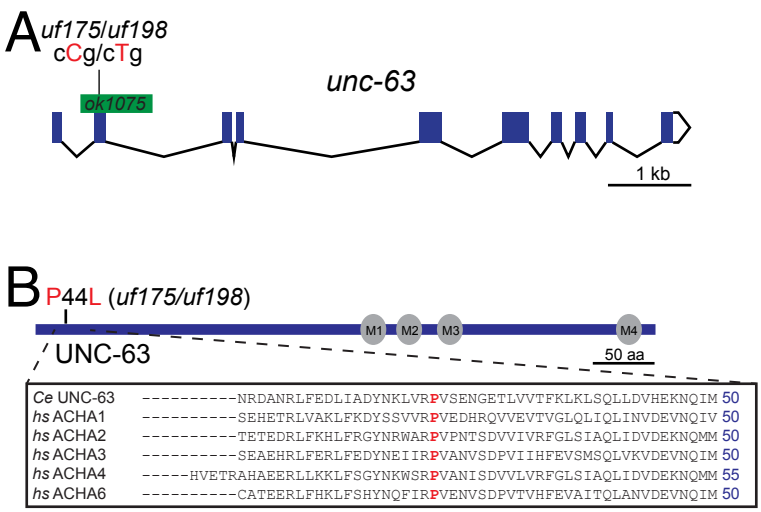
A
uf175/uf198
cCg/cTg
ok1075
unc-63
1 kb
B
P44L (uf175/uf198)
M1
M2
M3
M4
UNC-63
50 aa
Ce UNC-63 ----------NRDANRLFEDLIADYNKLVRPVSENGETLVVTFKLKLSQLLDVHEKNQIM 50
hs ACHA1 ----------SEHETRLVAKLFKDYSSVVRPVEDHRQVVEVTVGLQLIQLINVDEVNQIV 50
hs ACHA2 ----------TETEDRLFKHLFRGYNRWARPVPNTSDVVIVRFGLSIAQLIDVDEKNQMM 50
hs ACHA3 ----------SEAEHRLFERLFEDYNEIIRPVANVSDPVIIHFEVSMSQLVKVDEVNQIM 50
hs ACHA4 -----HVETRAHAEERLLKKLFSGYNKWSRPVANISDVVLVRFGLSIAQLIDVDEKNQMM 55
hs ACHA6 ----------CATEERLFHKLFSHYNQFIRPVENVSDPVTVHFEVAITQLANVDEVNQIM 50

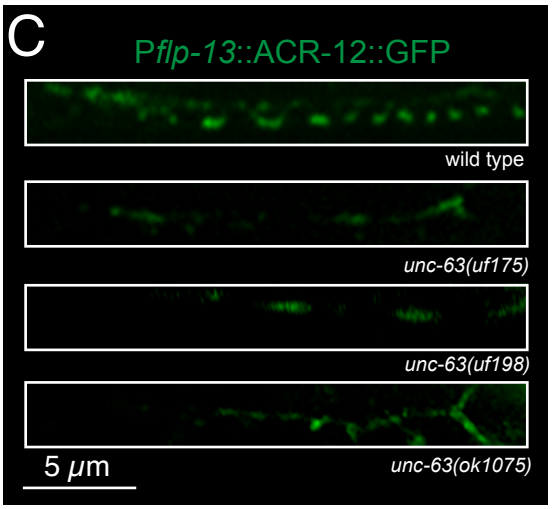
C
Pflp-13::ACR-12::GFP
wild type
unc-63(uf175)
unc-63(uf198)
5 µm
unc-63(ok1075)

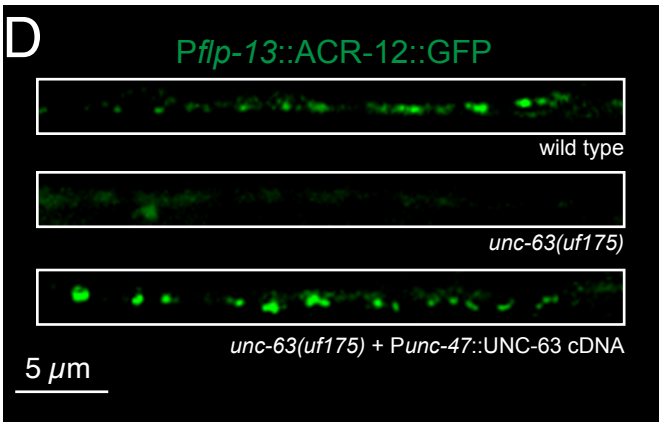
D
Pflp-13::ACR-12::GFP
wild type
unc-63(uf175)
unc-63(uf175) + Punc-47::UNC-63 cDNA
5 µm

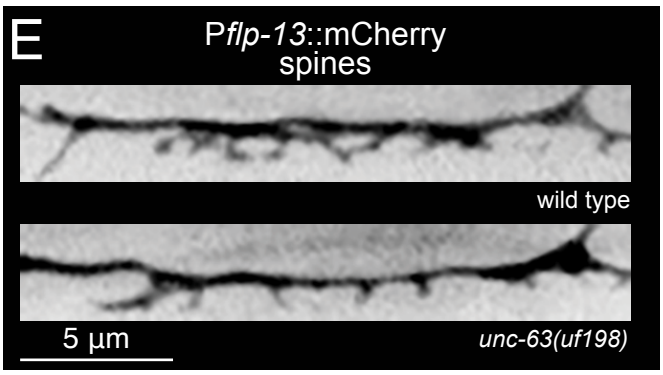
E
Pflp-13::mCherry
spines
wild type
5 µm
unc-63(uf198)

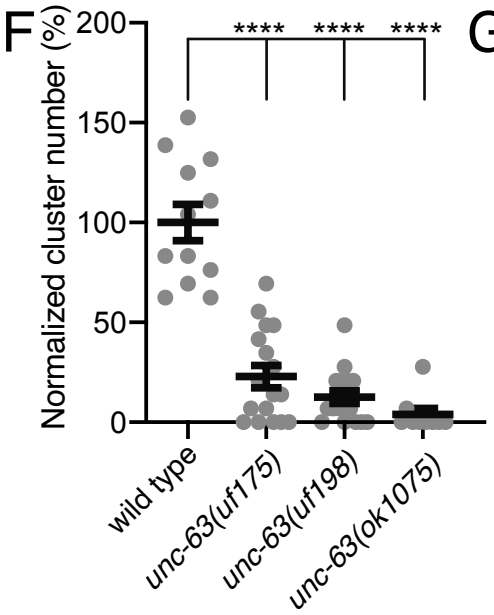
F
Normalized cluster number (%)
200
150
100
50
0
****
****
****
wild type
unc-63(uf175)
unc-63(uf198)
unc-63(ok1075)

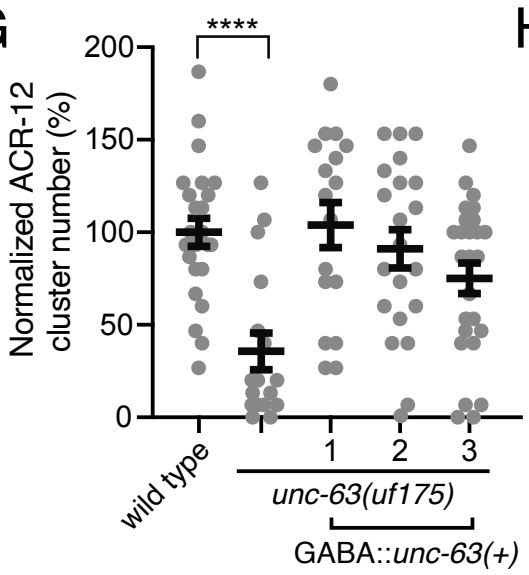
G
Normalized ACR-12
cluster number (%)
200
150
100
50
0
****
wild type
1
2
3
unc-63(uf175)
GABA::unc-63(+)

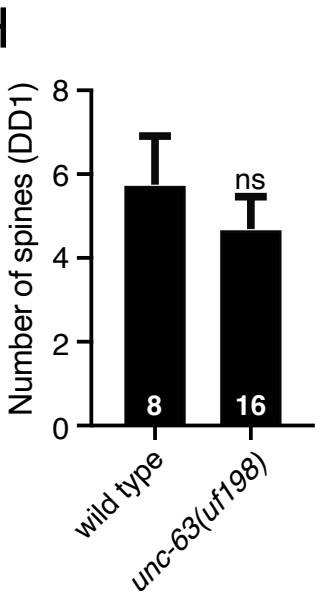
H
Number of spines (DD1)
8
6
4
2
0
ns
8
16
wild type
unc-63(uf198)

Figure 2. Mutation of a highly conserved proline residue near the N-terminus disrupts ACR-12 localization in DD motor neurons.

A. Domain structure of UNC-63. Transmembrane domains (TM) and *unc-63(uf175/uf198)* alleles are shown. Green line indicates sequence deletion in *unc-63(ok1075)* allele.

B. Transcript of *unc-63* with annotated *unc-63* alleles Sequence alignments of UNC-63 across species are detailed in box. The red "P" indicates the *unc-63(uf175/uf198*) mutation, a highly conserved proline in *C. elegans*, *Drosophila melanogaster*, and *Homo sapiens*.

C. Confocal images of DD1 ACR-12 localization (P*flp-13*::ACR-12) in wild type, *unc-63(ufl175)*, *unc-63(uf198)* and *unc-63(ok1075)* animals. Scale bar 5 µm.

D. Confocal images of DD1 ACR-12 localization (Pflp-13::ACR-12) in wild type, *unc-63(ufl175)* and GABAergic specific *unc-63(+)* rescue of *unc-63(uf175)* animals. Scale bar 5µm.

E. Representative confocal images of DD1 spines (P*flp-13*::mCherry) in wild type and *unc-63 (uf198)* animals.

F. ACR-12 cluster number is decreased in *unc-63* alleles. Mean ± SEM. One-way ANOVA with Dunnett's multiple comparisons test, **** $p<0.0001$ One-way ANOVA with Dunnett's multiple comparisons test.

G. ACR-12 clusters are rescued in three independent lines of GABAergic *unc-63 cDNA* rescue in *unc-63(uf175)* animals. Mean ± SEM. One-way ANOVA with Dunnett's multiple comparisons test, **** $p<0.0001$.

H. Spine number is not significantly different in *unc-63(uf198)* animals. Mean ± SEM. ns, not significant. Numbers indicate the number of animals quantified.

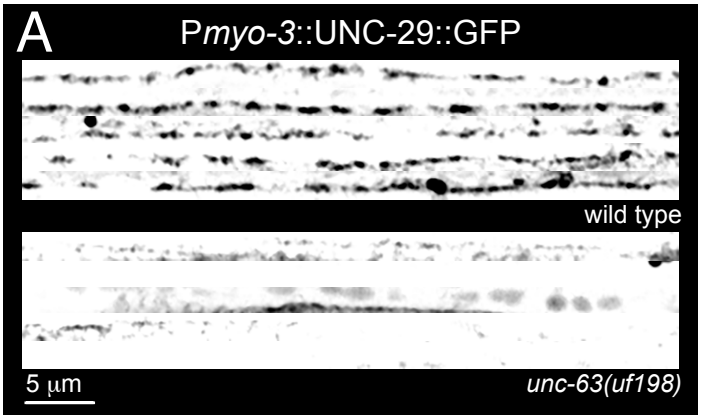
A
Pmyo-3::UNC-29::GFP
wild type
5 µm
unc-63(uf198)

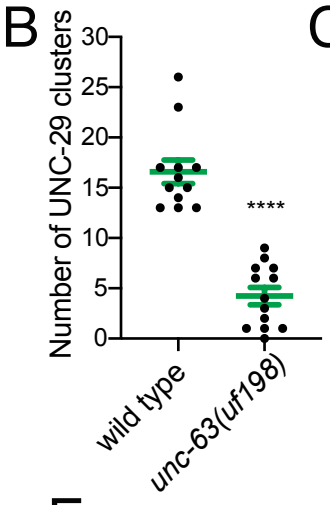
B
Number of UNC-29 clusters
30
25
20
15
10
5
0
****
wild type
unc-63(uf198)

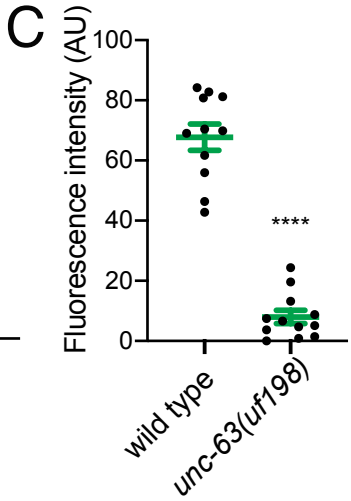
C
Fluorescence intensity (AU)
100
80
60
40
20
0
****
wild type
unc-63(uf198)

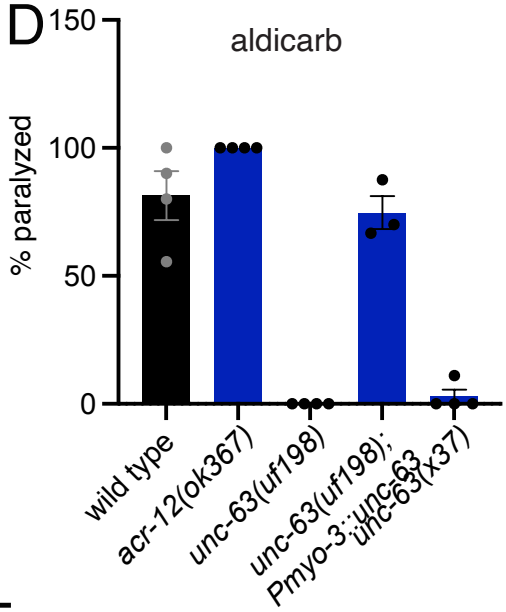
D
aldicarb
% paralyzed
150
100
50
0
wild type
acr-12(ok367)
unc-63(uf198)
unc-63(uf198);
Pmyo-3::unc-63
unc-63(x37)

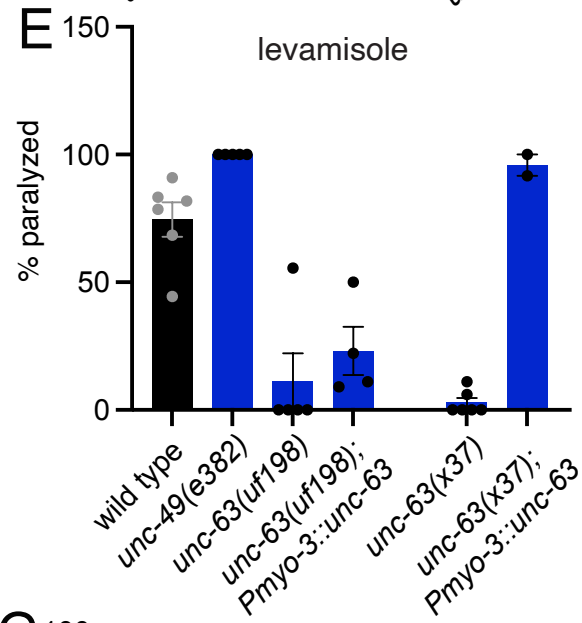
E
levamisole
% paralyzed
150
100
50
0
wild type
unc-49(e382)
unc-63(uf198)
unc-63(uf198);
Pmyo-3::unc-63
unc-63(x37)
unc-63(x37);
Pmyo-3::unc-63

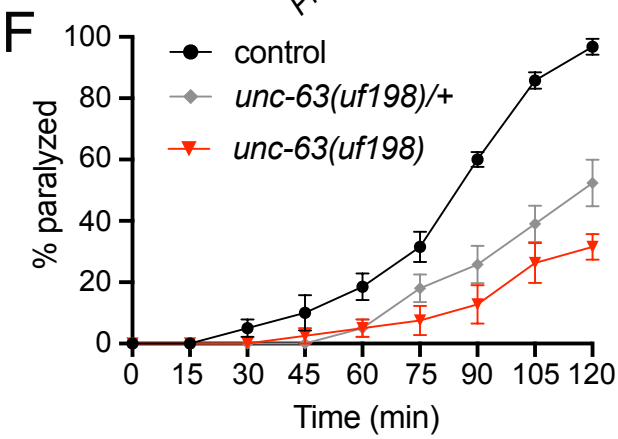
F
% paralyzed
100
80
60
40
20
0
control
unc-63(uf198)/+
unc-63(uf198)
0
15
30
45
60
75
90
105
120
Time (min)

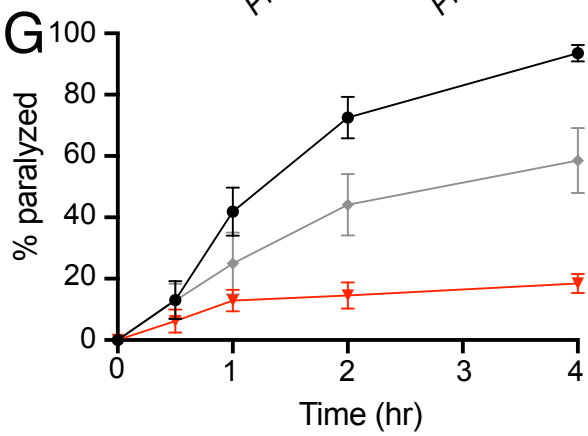
G
% paralyzed
100
80
60
40
20
0
0
1
2
3
4
Time (hr)

Figure. 3 The UNC-63 P44L substitution disrupts neuromuscular synapse organization and presents resistance to aldicarb and levamisole.

A) Representative confocal images of a ventral nerve cords in five wild type and *unc-63(uf198)* mutants expressing P*myo-3*::UNC-29::GFP (muscle AChRs).

(B-C) Number and fluorescence intensity of UNC-29 clusters is significantly decreased in *unc-63(uf198)* animals. Mean ± SEM. Student's t-test, **** $p<0.0001$.

(D-E) Quantification of % animals paralyzed upon exposure to aldicarb (D) and levamisole (E). *unc-63(uf198)* animals are resistant to aldicarb and levamisole. Muscle expression of *unc-63*+ failed to fully rescue phenotype.

(F-G) Animals heterozygous for *unc-63(uf198)* (grey) paralyze slower on aldicarb and levamisole than wild type controls (black) with *ufEx1685* and paralyze faster than homozygous *unc-63(uf198)* animals (red), suggesting the *unc-63(uf198)* may be semi-dominant.

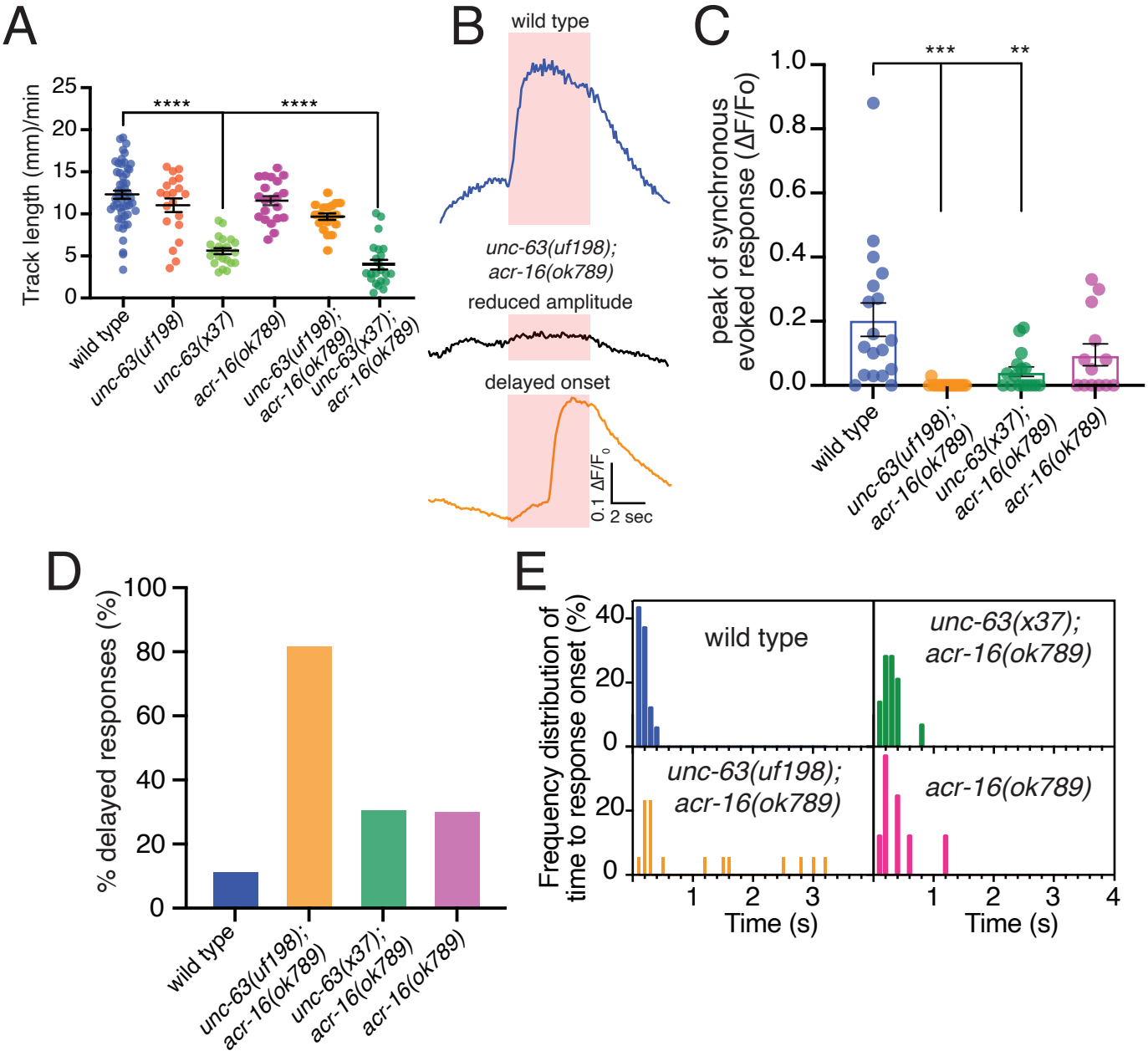
A
Track length (mm)/min
25
20
15
10
5
0
****
****
wild type
unc-63(uf198)
unc-63(x37)
acr-16(ok789)
unc-63(uf198); acr-16(ok789)
unc-63(x37); acr-16(ok789)
B
wild type
unc-63(uf198); acr-16(ok789)
reduced amplitude
delayed onset
0.1 ΔF/F0
2 sec
C
peak of synchronous evoked response (ΔF/Fo)
1.0
0.8
0.6
0.4
0.2
0.0
***
**
wild type
unc-63(uf198); acr-16(ok789)
unc-63(x37); acr-16(ok789)
D
% delayed responses (%)
100
80
60
40
20
0
wild type
unc-63(uf198); acr-16(ok789)
unc-63(x37); acr-16(ok789)
E
Frequency distribution of time to response onset (%)
40
20
0
wild type
unc-63(x37); acr-16(ok789)
unc-63(uf198); acr-16(ok789)
acr-16(ok789)
1
2
3
4
Time (s)
Time (s)

Figure. 4 *unc-63(uf198)* mutation produces mild behavior deficits and more severe disruption of neuromuscular responses

A. *unc-63(uf198)* animals move similar distances compared to wild type, *acr-16(ok789)* and *unc-63(uf198); acr-16(ok789)* animals; whereas *unc-63(x37)* and *unc-63(x37); acr-16(ok789)* animals move significantly less. Mean ± SEM. One-way ANOVA with Dunnett's multiple comparisons test, **** $p<0.0001$.

B. Representative evoked responses in wild type and *unc-63(uf198); acr-16(ok789)* animals. Note the two distinct types of responses (reduced amplitude and delayed onset responses) in the *unc-63(uf198)* animals. Red shading indicates the duration of the cholinergic optogenetic stimulation.

C. Quantification of the peak evoked synchronous responses for the indicated genotypes. Mean ± SEM. One-way ANOVA with Dunnett's multiple comparisons test, *** $p<0.001$; ** $p<0.01$.

D. Proportion of delayed onset responses calculated for the indicated genotypes. Note the high proportion of delayed onset responses in *unc-63(uf198)* animals.

E. Frequency distribution of the delay time to onset of evoked responses (delay calculated from the onset of the optogenetic stimulus) for the indicated genotypes. Note the significantly longer delay times in *unc-63(uf198)* animals.

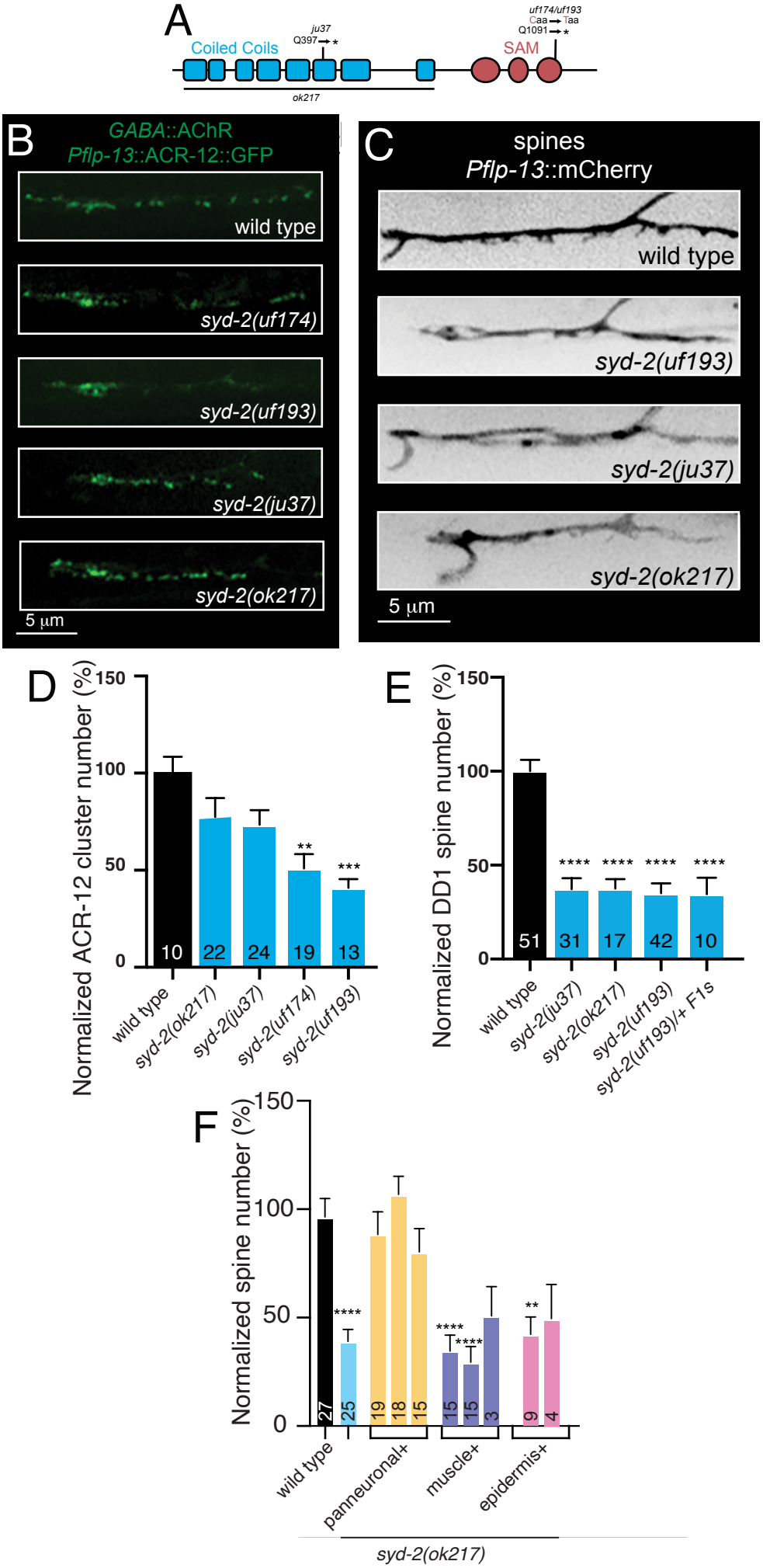
A
Coiled Coils
ju37
Q397 → *
uf174/uf193
Caa → Taa
Q1091 → *
SAM
ok217
B
GABA::AChR
Pflp-13::ACR-12::GFP
wild type
syd-2(uf174)
syd-2(uf193)
syd-2(ju37)
syd-2(ok217)
5 µm
C
spines
Pflp-13::mCherry
wild type
syd-2(uf193)
syd-2(ju37)
syd-2(ok217)
5 µm
D
Normalized ACR-12 cluster number (%)
150
100
50
0
10
22
24
19
13
**
***
wild type
syd-2(ok217)
syd-2(ju37)
syd-2(uf174)
syd-2(uf193)
E
Normalized DD1 spine number (%)
150
100
50
0
51
31
17
42
10
****
****
****
****
wild type
syd-2(ju37)
syd-2(ok217)
syd-2(uf193)
syd-2(uf193)/+ F1s
F
Normalized spine number (%)
150
100
50
0
27
25
19
18
15
15
15
3
9
4
****
****
****
**
wild type
panneuronal+
muscle+
epidermis+
syd-2(ok217)

Figure 5. The *syd-2(uf193)* mutation disrupts spine formation.

A. Domain structure of SYD-2. Coiled-coils (blue) and SAM domains (red) are shown. Black horizontal line indicates sequence deletion. Reference alleles *ju37* and *ok217* disrupt coiled coils domain while the screen isolated *uf174* and CRISPR engineered *uf193* alleles cause a stop (*) in the SAM domain.

B. Confocal images of DD1 ACR-12/AChR localization (P*flp-13*::ACR-12:GFP) in wildtype, screen isolate *syd-2(uf174)*, CRISPR engineered *syd-2(uf193)*, *syd-2(ju37)* and *syd-2(ok217)* animals. Scale bar 5µm.

C. Confocal images of DD1 spines (P*flp-13*::mCherry) in wild type, CRISPR engineered *syd-2(uf193),* s*yd-2(ju37)* and *syd-2(ok217)* animals. Scale bar 5µm.

D. Quantification of ACR-12/AChR clusters in the indicated *syd-2* alleles. Mean +SEM. One-way ANOVA, Dunnett's multiple comparison test, ** <p<0.01, *** p<0.001. Numbers indicate the number of animals quantified.

E. Quantification of DD1 spine number in indicated genotypes. Mean + SEM. One-way ANOVA, Dunnett's multiple comparison test. **** p<0.0001. Numbers indicate the number of animals quantified.

F. Quantification of DD1 neuron normalized spine number for the genotypes indicated. Mean ± SEM. One-way ANOVA, Dunnett's multiple comparison test. **** p<0.0001, ** p<0.01 compared to wild type. Numbers indicate number of animals quantified.

Supplementary Material and Tables

Table 1. Strains used in this study

GENOTYPE	STRAIN	DESCRIPTION
ufIs126	IZ1905	*Pflp-13::ACR-12::GFP + Plgc-11:mCherry*
ufIs128	IZ1464	*Pflp-13::mCherry + Plcgc-11::mCherry*
unc-14(uf169) 10X outcross	IZ3020	
unc-14(uf169); ufIs126	IZ2498	
unc-14(uf169); ufIs128	IZ2802	
unc-14(uf169); ufIs126; ufEx2069	IZ2790	*PCR amplified genomic unc-14 rescue*
unc-14(uf169); ufEx1922	IZ4534	*ufEx1922 = Pref-1::unc-14 cDNA (pJR14 @ 10 ng/µL + Pinx-6::GFP (pDO125 @ 50 ng/µL)*
unc-14(uf169); ufEx1249	IZ3020	*ufEx1249 = Pmyo-3::unc-14 cDNA-yk1203h04 (pDO13 @ 10 ng/µL) + Punc-122::GFP(50 ng/µL)*
unc-14(uf169); ufEx1156	IZ2906	*ufEx1156 = Punc-47:unc-14 cDNA-yk1203h04 (pDO17 @ 10 ng/µL) + Punc-122::GFP (50 ng/µL)*
unc-14(uf169); ufEx1173	IZ2906	*ufEx1173 = Punc-17Beta::unc-14 cDNA (pDO15 @ 10 ng/µL) + Punc-122::GFP (50 ng//µL)*
unc-14(e57)	CB57	
unc-14(e57); ufIs126	IZ1546	
unc-63(uf175); ufIs126	IZ2438	
unc-63(uf175); ufIs126; ufEx1104		*ufEx1104 = Punc-47::unc-63 cDNA (pAP59) @ 30 ng/µL + Punc-122::GFP @ 50 ng/µL*
unc-63(uf198)	IZ3558	

unc-63(uf198); ufIs126	IZ3917	
unc-63(uf198); ufIs128	IZ3714	
unc-63(uf198); ufIs2	IZ3753	*ufIs2 = Pmyo-3::unc-29::GFP (pDM956) + lin-15(+) (pJM23)*
unc-63(uf198); ufEx1907	IZ4494	*ufEx1907 = Pmyo-3::unc-63 (pAP212 @ 25 ng/µL) + Pinx-6::GFP (pDO125 @ 50 ng/µL)*
unc-63(x37); ufEx1907	IZ4494	
unc-63(ok1075)	VC731	
unc-63(ok1075); ufIs126	IZ1427	
acr-12(ok367)	IZ241	
zfEx813; ufIs157	IZ4568	*zfEx813 = Pmyo-3::GCaMP6s::SL2::mCherry (50 ng/µL); ufIs157 = Pacr-2::Chrimson (pRB2 @ 50 ng/µL)*
unc-63(uf198); acr-16(ok789); zfEx813; ufIs157	IZ4607	
unc-63(x37); acr-16(ok789); zfEx813; ufIs157	IZ4596	
acr-16(ok789); zfEx813; ufIs157	IZ4611	
syd-2(uf174)	IZ3341	
syd-2(uf174); ufIs126	IZ2321	
syd-2(uf193)	IZ3356	
syd-2(uf193); ufIs126	IZ3419	
syd-2(uf193); ufIs128	IZ3429	
syd-2(ju37)	CZ900	
syd-2(ju37); ufIs126	IZ3028	
syd-2(ju37); ufIs128	IZ3043	

syd-2(ok217)	ZM607	
syd-2(ok217); ufIs126	IZ2984	
syd-2(ok217); ufIs128	IZ2983	
syd-2(ok217); ufIs128; ufEx1430	IZ2983	*ufEx1430 = Prgef-1::syd-2 cDNA (pDO63 @ 10 ng/µL) + Punc-122::GFP (50 ng/µL)*
syd-2(ok217); ufIs128; ufEx1342	IZ3266	*Pmyo-3::syd-2cDNA (pDO33 @10ng/µL) + Punc-122::GFP (50 ng/µL)*
syd-2(ok217); ufIs128; ufEx1343	IZ3267	*Pelt-3::syd-2cDNA (pDO36 @10ng/µL) + Punc-122::GFP (50 ng/µL)*

Table 2. Plasmids used in this study

unc-14 promoter	pENTR-5'-22	For *unc-14* rescue, the *unc-14* genomic region including ~2.9 kb upstream from the ATG was amplified from N2 genomic DNA using primers OMF2079 and OMF2080, and ligated into pENTR D-TOPO using CACC overhang ligation to create pENTR-5'-22.
unc-14 transcriptional reporter (P*unc-14::mCherry*)	pDO22	pENTR-5'-22 was recombined with pDest-17 (mCherry) to create pDO22 (P*unc-14*::mCherry).
syd-2 promoter	pENTR-44	generated by amplifying the *syd-2* promoter region (3.2 kb) from N2 genomic DNA using primers OMF2358 and OMF2359 and ligating into pENTR-D-TOPO to create pENTR-44 (P*syd-2*).

syd-2 cDNA	pDest-159	*syd-2* cDNA was RT-PCR amplified from N2 RNA using primers OMF2336 and OMF2337, and ligated into NheI/NgoMIV digested pDest-150 to create pDest-159
syd-2 transcriptional reporter	pDO49	pENTR-44 was recombined with pDest-16 to create pDO49.
P*unc-47*::*syd-2* cDNA	pDO31	pDO31 (P*unc-47*::*syd-2* cDNA) was created by recombining pDest-159 with pENTR-P*unc-47*
P*unc-17β*::*syd-2* cDNA	pDO29	pDO29 (P*unc-17β*::*syd-2* cDNA) was created by recombining pDest-159 with pENTR-P*unc-17β*
P*myo-3*::*syd-2* cDNA	pDO33	pDO33 (P*myo-3*::*syd-2* cDNA) was created by

		recombining pDest-159 with pENTR-P*myo-3*.
P*elt-3::syd-2* cDNA	pDO36	pDO36 (P*elt-3::syd-2* cDNA) was created by recombining pDest-159 with pENTR-34 (P*elt-3*).

Primers used in this study

Primer name	Description	Sequence 5'→ 3'
OMF 2079	*unc-14* genomic amplification	CACCTCTCTTTCCAGGTGTACG
OMF 2080	*unc-14* genomic amplification	CACCTTTGGTGGAAGAATTGAGGGA
OMF2336	*syd-2* cDNA amplification	ATTAGCTAGCAAAAATGAGCTACAGCAATGGAAACATAAAT
OMF2337	*syd-2* cDNA amplification	GCTAGCCGGCCTAGGTATATAAATGAAACTCGTAGGA
OMF2358	*syd-2* promoter amplification	CACCgcctctgggcatgctgattggcattttcg
OMF2359	*syd-2* promoter amplification	CACCatttctgaaacagattaaaattgataac

Information on generated CRISPR strains

All CRISPR/Cas9 used in these studies were generated as described (Arribere et al., 2014).

unc-63(uf198)

The gRNA plasmids were made as previously described (Arribere et al., 2014). Target sequences were selected on exon 2 of *unc-63*. Forward and reverse oligonucleotides were designed to contain the target sequence and overhangs compatible with *Bsa*I sites in plasmid Forward and reverse oligonucleotides were designed to contain the target sequence and overhangs compatible with *BsaI* sites in plasmid pPP13, a modified version of pRB1017 (Arribere et al., 2014) were the sgRNA scaffold was replaced with the sgRNA(F+E) scaffold (Ward, 2015). Forward and reverse oligonucleotides were annealed and ligated into pPP13 cut with *Bsa*I to create the gRNA plasmids. Plasmids were confirmed by sequencing with M13 reverse primer. A DNA mixture of pDD162 (P*eft-3*::Cas-9) (50 ng/µL), the gRNA plasmids (40 ng/µL each), pPP15 (50 ng/µL) (dpy-10 target, a modified version of pJA58 were the sgRNA scaffold was replaced with the sgRNA(F+E) scaffold (Ward, 2015), the ssODN repair template for *dpy10(cn64)* (20 ng/µL) and the ssODN repair template for *unc-63* (Donor uf175) (80ng/µL) was prepared in injection buffer (Arribere et al., 2014) and injected into N2 worms. Donor uf175 contains a point mutation cCg/cTg resulting in a P/L amino acid change and a point mutation to eliminate an *AgeI* site for screening of mutants. Mutations in the *dpy-10* gene were used as a CRISPR co-conversion marker. The F1 progeny were screened for Rol and Dpy phenotypes 3–4 days after injection and then for target mutation in the *unc-63* coding region using PCR and *AgeI* digest. The *unc-63(uf198)* mutant contains a cCg/cTg point mutation at codon 44 P/L.

syd-2(uf193)

The gRNA plasmids were made as previously described (Arribere et al., 2014). Target sequences were selected on exon 18 of *syd-2*. Forward and reverse oligonucleotides were designed to contain the target sequence and overhangs compatible with *Bsa*I sites in plasmid pPP13, a

modified version of pRB1017 (Arribere et al., 2014) were the sgRNA scaffold was replaced with the sgRNA(F+E) scaffold (Ward, 2015). Forward and reverse oligonucleotides were annealed and ligated into pPP13 cut with *Bsa*I to create the gRNA plasmids. Plasmids were confirmed by sequencing with M13 reverse primer. A DNA mixture of pDD162 (Peft-3::Cas-9) (50 ng/µL), the gRNA plasmids (50 ng/µL each), pPP15 (50 ng/µL) (dpy-10 target, a modified version of pJA58 were the sgRNA scaffold was replaced with the sgRNA(F+E) scaffold (Ward, 2015), the ssODN repair template for *dpy10(cn64)* (20 ng/µL) and the ssODN repair template for syd-2 (Donor uf174) (50ng/µL) was prepared in injection buffer (Arribere et al., 2014) and injected into N2 worms. Donor uf174 contains a point mutation Caa/Taa resulting in a Q/stop change and the generation if an *AflII* site for screening of mutants. Mutations in the *dpy-10* gene were used as a CRISPR co-conversion marker. The F1 progeny were screened for Rol and Dpy phenotypes 3–4 days after injection and then for target mutation in the *usyd-2* coding region using PCR and *AgeI* digest. The *syd-2(uf193)* mutant contains a point mutation CCA/TAA resulting in a Q/stop at codon 1091.

References

Albuquerque EX, Pereira EFR, Alkondon M, Rogers SW (2009) Mammalian Nicotinic Acetylcholine Receptors: From Structure to Function. Physiol Rev 89:73–120.

Arribere JA, Bell RT, Fu BXH, Artiles KL, Hartman PS, Fire AZ (2014) Efficient Marker-Free Recovery of Custom Genetic Modifications with CRISPR/Cas9 in Caenorhabditis elegans. Genetics 198:837–846.

Brenner S (1974) THE GENETICS OF CAENORHABDITIS ELEGANS. Genetics 77:71–94.

Callebaut I, Jean, Gunzburg de, Goud B, Mornon J-P (2001) RUN domains: a new family of domains involved in Ras-like GTPase signaling. Trends Biochem Sci 26:79–83.

Chaya T, Patel S, Smith EM, Lam A, Miller EN, Clupper M, Kervin K, Tanis JE (2021) A C. elegans genome-wide RNAi screen for altered levamisole sensitivity identifies genes required for muscle function. G3 11:jkab047.

Cuentas-Condori A, Mulcahy B, He S, Palumbos S, Zhen M, Miller DM (2019) C. elegans neurons have functional dendritic spines. eLife 8:e47918.

Culetto E, Baylis HA, Richmond JE, Jones AK, Fleming JT, Squire MD, Lewis JA, Sattelle DB (2004) The Caenorhabditis elegans unc-63 Gene Encodes a Levamisole-sensitive Nicotinic Acetylcholine Receptor α Subunit. J Biol Chem 279:42476–42483.

Dai Y, Taru H, Deken SL, Grill B, Ackley B, Nonet ML, Jin Y (2006) SYD-2 Liprin-α organizes presynaptic active zone formation through ELKS. Nat Neurosci 9:1479–1487.

Dash B, Li MD, Lukas RJ (2014) Roles for N-terminal Extracellular Domains of Nicotinic Acetylcholine Receptor (nAChR) β3 Subunits in Enhanced Functional Expression of Mouse α6β2β3- and α6β4β3-nAChRs*. J Biol Chem 289:28338–28351.

Doitsidou M, Jarriault S, Poole RJ (2016) Next-Generation Sequencing-Based Approaches for Mutation Mapping and Identification in Caenorhabditis elegans. Genetics 204:451–474.

Dunah AW, Hueske E, Wyszynski M, Hoogenraad CC, Jaworski J, Pak DT, Simonetta A, Liu G, Sheng M (2005) LAR receptor protein tyrosine phosphatases in the development and maintenance of excitatory synapses. Nat Neurosci 8:458–467.

Emperador-Melero J, Wong MY, Wang SSH, Nola G de, Nyitrai H, Kirchhausen T, Kaeser PS (2021) PKC-phosphorylation of Liprin-α3 triggers phase separation and controls presynaptic active zone structure. Nat Commun 12:3057.

Fouquet W, Owald D, Wichmann C, Mertel S, Depner H, Dyba M, Hallermann S, Kittel RJ, Eimer S, Sigrist SJ (2009) Maturation of active zone assembly by Drosophila Bruchpilot. J Cell Biol 186:129–145.

Francis MM, Evans SP, Jensen M, Madsen DM, Mancuso J, Norman KR, Maricq AV (2005) The Ror Receptor Tyrosine Kinase CAM-1 Is Required for ACR-16-Mediated Synaptic Transmission at the C. elegans Neuromuscular Junction. Neuron 46:581–594.

Geitmann M, Retra K, Kloe GE de, Homan E, Smit AB, Esch IJP de, Danielson UH (2010) Interaction Kinetic and Structural Dynamic Analysis of Ligand Binding to Acetylcholine-Binding Protein. Biochemistry 49:8143–8154.

Gottschalk A, Almedom RB, Schedletzky T, Anderson SD, Yates JR, Schafer WR (2005) Identification and characterization of novel nicotinic receptor-associated proteins in Caenorhabditis elegans. Embo J 24:2566–2578.

Hallam SJ, Goncharov A, McEwen J, Baran R, Jin Y (2002) SYD-1, a presynaptic protein with PDZ, C2 and rhoGAP-like domains, specifies axon identity in C. elegans. Nat Neurosci 5:1137–1146.

Hansen SB, Talley TT, Radić Z, Taylor P (2004) Structural and Ligand Recognition Characteristics of an Acetylcholine-binding Protein from Aplysia californica *. J Biol Chem 279:24197–24202.

Jones AK, Rayes D, Al-Diwani A, Maynard TPR, Jones R, Hernando G, Buckingham SD, Bouzat C, Sattelle DB (2011) A Cys-loop Mutation in the Caenorhabditis elegans Nicotinic Receptor Subunit UNC-63 Impairs but Does Not Abolish Channel Function*. J Biol Chem 286:2550–2558.

Jorgensen EM, Mango SE (2002) The art and design of genetic screens: Caenorhabditis elegans. Nat Rev Genet 3:356–369.

Jospin M, Bonneau B, Lainé V, Bessereau J-L (2022) An extracellular scaffolding complex confers unusual rectification upon an ionotropic acetylcholine receptor in C. elegans. Proc Natl Acad Sci 119:e2113545119.

Kittelmann M, Hegermann J, Goncharov A, Taru H, Ellisman MH, Richmond JE, Jin Y, Eimer S (2013) Liprin-α/SYD-2 determines the size of dense projections in presynaptic active zones in C. elegans. J Cell Biol 203:849–863.

LaConte LEW, Chavan V, Liang C, Willis J, Schönhense E-M, Schoch S, Mukherjee K (2016) CASK stabilizes neurexin and links it to liprin-α in a neuronal activity-dependent manner. Cell Mol Life Sci 73:3599–3621.

Larsch J, Flavell SW, Liu Q, Gordus A, Albrecht DR, Bargmann CI (2015) A Circuit for Gradient Climbing in C. elegans Chemotaxis. Cell Reports 12:1748–1760.

Léna C, Changeux J-P (1997) Role of Ca 2+ Ions in Nicotinic Facilitation of GABA Release in Mouse Thalamus. J Neurosci 17:576–585.

McDonald NA, Fetter RD, Shen K (2020) Assembly of synaptic active zones requires phase separation of scaffold molecules. Nature:1–5.

Minevich G, Park DS, Blankenberg D, Poole RJ, Hobert O (2012) CloudMap: A Cloud-Based Pipeline for Analysis of Mutant Genome Sequences. Genetics 192:1249–1269.

Ogura K, Goshima Y (2006) The autophagy-related kinase UNC-51 and its binding partner UNC-14 regulate the subcellular localization of the Netrin receptor UNC-5 in Caenorhabditis elegans. Development 133:3441–3450.

Ogura K, Shirakawa M, Barnes TM, Hekimi S, Ohshima Y (1997) The UNC-14 protein required for axonal elongation and guidance in Caenorhabditis elegans interacts with the serine/threonine kinase UNC-51. Genes Dev 11:1801–1811.

Oliver D, Ramachandran S, Philbrook A, Lambert CM, Nguyen KCQ, Hall DH, Francis MM (2022) Kinesin-3 mediated axonal delivery of presynaptic neurexin stabilizes dendritic spines and postsynaptic components. Plos Genet 18:e1010016.

Owald D, Fouquet W, Schmidt M, Wichmann C, Mertel S, Depner H, Christiansen F, Zube C, Quentin C, Körner J, Urlaub H, Mechtler K, Sigrist SJ (2010) A Syd-1 homologue regulates pre- and postsynaptic maturation in Drosophila. J Cell Biol 188:565–579.

Owald D, Khorramshahi O, Gupta VK, Banovic D, Depner H, Fouquet W, Wichmann C, Mertel S, Eimer S, Reynolds E, Holt M, Aberle H, Sigrist SJ (2012) Cooperation of Syd-1 with Neurexin synchronizes pre- with postsynaptic assembly. Nat Neurosci 15:1219–1226.

Patel MR, Lehrman EK, Poon VY, Crump JG, Zhen M, Bargmann CI, Shen K (2006) Hierarchical assembly of presynaptic components in defined C. elegans synapses. Nat Neurosci 9:1488–1498.

Philbrook A, Ramachandran S, Lambert CM, Oliver D, Florman J, Alkema MJ, Lemons M, Francis MM (2018) Neurexin directs partner-specific synaptic connectivity in C. elegans. Elife 7:e35692.

Sakamoto R, Byrd DT, Brown HM, Hisamoto N, Matsumoto K, Jin Y (2005) The Caenorhabditis elegans UNC-14 RUN Domain Protein Binds to the Kinesin-1 and UNC-16 Complex and Regulates Synaptic Vesicle Localization. Mol Biol Cell 16:483–496.

Schindelin J, Arganda-Carreras I, Frise E, Kaynig V, Longair M, Pietzsch T, Preibisch S, Rueden C, Saalfeld S, Schmid B, Tinevez J-Y, White DJ, Hartenstein V, Eliceiri K, Tomancak P, Cardona A (2012) Fiji: an open-source platform for biological-image analysis. Nat Methods 9:676–682.

Serra-Pagès C, Medley QG, Tang M, Hart A, Streuli M (1998) Liprins, a Family of LAR Transmembrane Protein-tyrosine Phosphatase-interacting Proteins*. J Biol Chem 273:15611–15620.

Spangler SA, Hoogenraad CC (2007) Liprin-α proteins: scaffold molecules for synapse maturation. Biochem Soc Trans 35:1278–1282.

Spangler SA, Schmitz SK, Kevenaar JT, Graaff E de, Wit H de, Demmers J, Toonen RF, Hoogenraad CC (2013) Liprin-α2 promotes the presynaptic recruitment and turnover of RIM1/CASK to facilitate synaptic transmission. J Cell Biol 201:915–928.

Stigloher C, Zhan H, Zhen M, Richmond J, Bessereau J-L (2011) The Presynaptic Dense Projection of the Caenorhabditis elegans Cholinergic Neuromuscular Junction Localizes Synaptic Vesicles at the Active Zone through SYD-2/Liprin and UNC-10/RIM-Dependent Interactions. J Neurosci 31:4388–4396.

Touroutine D, Fox RM, Stetina SEV, Burdina A, Miller DM, Richmond JE (2005) acr-16 Encodes an Essential Subunit of the Levamisole-resistant Nicotinic Receptor at the Caenorhabditis elegans Neuromuscular Junction. J Biol Chem 280:27013–27021.

Tzartos SJ, Cung MT, Demange P, Loutrari H, Mamalaki A, Marraud M, Papadouli I, Sakarellos C, Tsikaris V (1991) The main immunogenic region (MIR) of the nicotinic acetylcholine receptor and the anti-MIR antibodies. Mol Neurobiol 5:1–29.

Wentzel C, Sommer JE, Nair R, Stiefvater A, Sibarita J-B, Scheiffele P (2013) mSYD1A, a Mammalian Synapse-Defective-1 Protein, Regulates Synaptogenic Signaling and Vesicle Docking. Neuron 78:1012–1023.

Wong MY, Liu C, Wang SSH, Roquas ACF, Fowler SC, Kaeser PS (2018) Liprin-α3 controls vesicle docking and exocytosis at the active zone of hippocampal synapses. Proc Natl Acad Sci 115:2234–2239.

Wyszynski M, Kim E, Dunah AW, Passafaro M, Valtschanoff JG, Serra-Pagès C, Streuli M, Weinberg RJ, Sheng M (2002) Interaction between GRIP and Liprin-α/SYD2 Is Required for AMPA Receptor Targeting. Neuron 34:39–52.

Yeh E, Kawano T, Weimer RM, Bessereau J-L, Zhen M (2005) Identification of Genes Involved in Synaptogenesis Using a Fluorescent Active Zone Marker in Caenorhabditis elegans. J Neurosci 25:3833–3841.

Yoshida H, Kitagishi Y, Okumura N, Murakami M, Nishimura Y, Matsuda S (2011) How do you RUN on? FEBS Lett 585:1707–1710.

Zhen M, Jin Y (1999) The liprin protein SYD-2 regulates the differentiation of presynaptic termini in C. elegans. Nature 401:371–375.